Structure of a flavin-binding plant photoreceptor domain: Insights into light-mediated signal transduction

Sean Crosson*† and Keith Moffat*†‡§

*Department of Biochemistry and Molecular Biology, ‡Center for Advanced Radiation Sources, and §Institute for Biophysical Dynamics, University of Chicago, 920 East 58th Street, Chicago, IL 60637

Edited by Vincent Massey, University of Michigan Medical School, Ann Arbor, MI, and approved January 3, 2001 (received for review October 31, 2000)

Phototropin, a major blue-light receptor for phototropism in seed plants, exhibits blue-light-dependent autophosphorylation and contains two light, oxygen, or voltage (LOV) domains and a serine/threonine kinase domain. The LOV domains share homology with the PER-ARNT-SIM (PAS) superfamily, a diverse group of sensor proteins. Each LOV domain noncovalently binds a single FMN molecule and exhibits reversible photochemistry *in vitro* when expressed separately or in tandem. We have determined the crystal structure of the LOV2 domain from the phototropin segment of the chimeric fern photoreceptor phy3 to 2.7-Å resolution. The structure constitutes an FMN-binding fold that reveals how the flavin cofactor is embedded in the protein. The single LOV2 cysteine residue is located 4.2 Å from flavin atom C(4a), consistent with a model in which absorption of blue light induces formation of a covalent cysteinyl-C(4a) adduct. Residues that interact with FMN in the phototropin segment of the chimeric fern photoreceptor (phy3) LOV2 are conserved in LOV domains from phototropin of other plant species and from three proteins involved in the regulation of circadian rhythms in *Arabidopsis* and *Neurospora*. This conservation suggests that these domains exhibit the same overall fold and share a common mechanism for flavin binding and light-induced signaling.

Light is one of the most important abiotic factors influencing plant growth and development. A wide range of phenomena including seed germination, pigment biosynthesis, floral induction, circadian rhythms, and phototropism is determined by the light environment of the plant (1). Control of these responses in higher plants is located primarily within specific wavelength bands in the red or blue regions of the visible spectrum that are perceived by different photoreceptors (2, 3). The bilin-binding phytochromes mediate responses to red and far-red light (4), whereas cryptochrome 1/cryptochrome 2 (5), a stomata-regulating blue-light receptor (6), and phototropin (nph1; ref. 7) mediate responses to blue light. Phototropin is a membrane-associated kinase that undergoes autophosphorylation in response to absorption of blue light and serves as a photoreceptor for phototropism (8, 9). Phototropin has been identified in several species including *Arabidopsis thaliana*, oat (*Avena sativa*), rice (*Oryza sativa*), and corn (*Zea mays*; ref. 7). A chimeric phototropin from the fern *Adiantum*, denoted phy3, contains an additional phytochrome domain at its N terminus (10). Unlike the strictly blue-light-controlled phototropic response seen in most plants, phototropism in *Adiantum* can be induced by either red or blue light and is postulated to be mediated by phy3 (11).

The domain structure of phototropin consists of a C-terminal serine/threonine kinase and two upstream light, oxygen, or voltage (LOV) domains that each bind a single molecule of FMN (12). These LOV1 and LOV2 domains, expressed singly or in tandem, undergo a fully reversible photocycle characterized by a photoinduced blue shift of three major bands that absorb in the blue, with spontaneous recovery of these bands in the dark (13). The spectrum of this blue-shifted state resembles that of a covalent C(4a) flavin-cysteinyl adduct (14), which suggested that the primary mechanism underlying light detection in phototropin is formation of a flavin-cysteinyl adduct in the LOV domains (13). Indeed, site-directed mutagenesis of a single cysteine in oat LOV1 and LOV2 does not hinder FMN binding but abolishes the photocycle (13).

LOV domains (7) form a subgroup of the larger PAS domain superfamily, a class of sensory proteins named after *Drosophila* period (*P*ER), vertebrate aryl hydrocarbon receptor nuclear translocator (*A*RNT), and *Drosophila* single-minded (*S*IM; refs. 15–18). In addition to their sensory functions, PAS domains have been reported to mediate protein–protein interactions (18). The PAS superfamily is characterized structurally by three helical segments flanking a five-stranded antiparallel β-sheet (19–23). The functionally diverse PAS domains are structurally diverse in their cofactor-binding properties. For example, cofactors found in PAS domains include: (*i*) 4-hydroxycinnamic acid covalently attached to the single cysteine in photoactive yellow protein (PYP; refs. 24 and 25); (*ii*) iron protoporphyrin IX covalently attached to a histidine residue in FixL (sensor protein in *Rhizobium* nitrogen fixation pathway; ref. 26); (*iii*) flavin adenine dinucleotide noncovalently bound to nitrogen fixation regulatory protein L and *Escherichia coli* aerotaxis sensor (27–29); and (*iv*) FMN noncovalently bound to phototropin (9, 12). Three crystal structures from the PAS-domain superfamily have been reported: the bacterial blue-light photosensor PYP (19, 20), the heme-binding domain of the rhizobial oxygen sensor FixL (21, 22), and the N-terminal domain of the human ether-a-go-go-related gene potassium channel (HERG; ref. 23). Notably, HERG contains no cofactor but retains the protein fold characteristic of PAS domains.

Here we report the three-dimensional structure of LOV2 from the phototropin module of *Adiantum* phy3 in the dark state, propose a general mechanism for its response to light, and extend this analysis to related proteins.

Materials and Methods

LOV2 Expression and Purification. A construct containing an N-terminal calmodulin-binding peptide (see ref. 12) and spanning amino acid residues 924 to 1,051 of phy3 LOV2 was expressed in

This paper was submitted directly (Track II) to the PNAS office.

Abbreviations: phy3, chimeric fern photoreceptor; LOV, light, oxygen, or voltage; PAS, a class of sensory proteins named after *Drosophila* period (*P*ER), vertebrate aryl hydrocarbon receptor nuclear translocator (*A*RNT), and *Drosophila* single-minded (*S*IM); PYP, photoactive yellow protein; FixL, sensor protein in *Rhizobium* nitrogen fixation pathway; HERG, human ether-a-go-go-related gene.

Data deposition: The atomic coordinates for phy3 LOV2 have been deposited in the Protein Data Bank, www.rcsb.org (PDB ID code 1G28).

†To whom reprint requests should be addressed. E-mail: scrosson@midway.uchicago.edu or moffat@cars.uchicago.edu.

The publication costs of this article were defrayed in part by page charge payment. This article must therefore be hereby marked "*advertisement*" in accordance with 18 U.S.C. §1734 solely to indicate this fact.

BIOCHEMISTRY

Table 1. Data and refinement statistics

Data	
Space group	P1
a, *b*, *c*, Å	44.89, 54.08, 70.62
α, β, γ, deg	93.32, 94.01, 90.01
Unique reflections	16249 to 2.73 Å
Test set	1179
Resolution/last shell, Å	40–2.73/2.78–2.73
I/σ(I)	14.3/1.6
R_{merge}*, %	11.5/48.9
Completeness, %	96.4/95.8
Overall redundancy	1.8
Refinement statistics	
R_{cryst}†	24.7
R_{free}‡	27.2
Wilson *B*, Å^2	20.6
B, Å^2	31.3
rmsd§ bond lengths, Å^2	0.010
rmsd§ bond angles, deg	1.4
Ramachandran distribution	
Most favored, %	85
Allowed, %	15
Outside allowed, %	0
Water molecules	51

*$R_{merge} = \Sigma_{hkl}\Sigma_i|AFI_i - \langle I\rangle|/\Sigma_{hkl}\Sigma_i I_i$, for all data $I/\sigma(I) > -3$.
†$R_{cryst} = \Sigma_{hkl}||F_{obs}| - |F_{calc}||/\Sigma_{hkl}|F_{obs}|$, includes all data.
‡R_{free} uses 6.7% of the data for the test set. Test set was selected using thin randomly chosen resolution shells (37, 38) to remove noncrystallographic symmetry relationships between reflections.
§rmsd, root-mean-square deviation.

E. coli BL21(DE3) cells. Expression was carried out in darkness for 4 h at 28°C in the presence of 750 μM isopropyl β-D-galactopyranoside (induction at OD_{600} = 0.4–0.5). Harvested cells were frozen overnight at −20°C, thawed, and lysed by sonication. The LOV2–calmodulin-binding peptide fusion protein was purified on calmodulin resin (Stratagene) according to manufacturer's instructions. After overnight dialysis at 4°C to remove excess salt, the calmodulin-binding peptide tag was cleaved with thrombin (Hematologic Technologies, Essex Junction, VT). LOV2 was purified further on fast-flow Sepharose Q (Amersham Pharmacia) by using an increasing NaCl gradient to separate thrombin, uncleaved protein, and calmodulin-binding peptide from LOV2. Purified phy3 LOV2 migrated as a single band of molecular mass 15,000 Da on SDS/PAGE and was concentrated in a high-pressure stirred ultrafiltration cell (YM3 membrane, Amicon). Protein stock used for crystallization was 9 mg/ml, as determined by using an extinction coefficient of 11.2 $mM^{-1}\cdot cm^{-1}$ at 450 nm (12), and remained in its ion-exchange elution buffer (20 mM Tris, pH 8.0/250 mM NaCl).

LOV2 Crystallization and X-Ray Data Collection. Crystals were grown in 8-μl hanging drops at 20°C by vapor diffusion against 50 mM Tris, pH 8.0/24% (wt/vol) PEG 5,000 monomethyl-ether/12% (vol/vol) glycerol and appeared in 2 weeks. Diffraction data were collected at room temperature from a triclinic crystal (400 × 400 × 80 μm) by using CuKα radiation from a rotating RU200 anode generator (Rigaku, Tokyo) and an R-AXIS IIC detector. Intensities were scaled and integrated by using DENZO and SCALEPACK (30). The crystal initially diffracted beyond 2.1 Å and belongs to the space group P_1 (Table 1).

Structure Determination. The structure of phy3 LOV2 was solved by molecular replacement with data in the resolution range of 10–3.5 Å by using the program AMORE (31) within the CCP4 package (32). Several models including HERG, PYP, and FixL were tried. The successful model was a partial polyalanine model based on residues 27–126 of HERG (PDB ID code 1BYW) that retained the 30 side chains conserved between HERG and phy3 LOV2. Successive translation searches in AMORE revealed four LOV2 domains per asymmetric unit. Then, 4-fold noncrystallographic symmetry-averaged maps generated by using the program DM in the CCP4 package revealed additional side-chain density for certain nonalanine residues. Density corresponding to the C-terminal β-strand and a plausible position for FMN also was evident thus confirming the correctness of the molecular replacement solution. The initial R_{cryst} for the molecular replacement model was 47%.

The structure was refined to 2.73 Å by using rigid-body, positional refinement, simulated annealing, and B-factor protocols in CNS (33). Tight 4-fold noncrystallographic symmetry restraints (300-kcal/mole/Å^2) were used during refinement. When refinement was run with less stringent restraints, R_{cryst} decreased slightly, but R_{free} increased, which suggested over fitting. Simulated-annealing omit maps of FMN and portions of the polypeptide chain were produced by setting omit atom-occupancy to zero in one monomer and running positional refinement and simulated annealing. All model building was carried out in O (34). The stereochemical quality of the final refined model was assessed by using PROCHECK (35), and structure figures were generated with RIBBONS (36). Details of the refinement are summarized in Table 1.

Structural and Sequence Alignment. Least-squares fits of the atomic coordinates of PAS domains PYP, FixL, and HERG (PDB ID codes 2PHY, 1DRM, and 1BYW, respectively) against our model of LOV2 used the CCP4 program LSQKAB. A multiple sequence alignment of LOV domains was generated by using CLUSTALW 1.8 within the BCM SEARCH LAUNCHER (39); sequences were displayed by using BOXSHADE. Space-filling model of phy3 LOV2 was generated by using GRASP (40).

Results and Discussion

Crystal Structure of LOV2. Crystals of purified LOV2 from *Adiantum* phy3 (Fig. 1*A*) were grown in both monoclinic and triclinic space groups. Monoclinic crystals diffracted to ≈2.0 Å but exhibited substantial static disorder. The structure of LOV2 was solved therefore from a single triclinic crystal that diffracted initially beyond 2.1 Å. After completion of data collection, resolution of the diffraction pattern had decreased to ≈3.0 Å. A self-rotation function showed four LOV2 domains per asymmetric unit arranged as two LOV2 dimers around local 2-fold axes. Dyad axes of the two LOV2 dimers were inclined to each other at 90°.

Residues 929 to 1,032 and the FMN cofactor were defined clearly in all four monomers within the asymmetric unit; these 104 residues constitute the PAS fold. However, we were unable to model any additional residues expressed from the LOV2 construct, because electron density is highly fragmented or absent at the termini of our model. Nevertheless, the excellent main- and side-chain electron density for residues 929–1,032 made model building and refinement straightforward. A simulated-annealing omit map of FMN from a single monomer in the asymmetric unit calculated at $\pm 3.5\sigma$ and $\pm 10\sigma$ confirms the quality of our maps (Fig. 2*A*), as do additional simulated-annealing omit-map calculations on several portions of the polypeptide (data not shown).

Previous work (7, 9, 10, 12, 13) described LOV domains as a subset of the PAS-domain superfamily contained in proteins regulated by state light, oxygen, or voltage here. Here, we restrict its definition structurally to a light-regulated FMN-binding domain present in all currently identified phototropins and phototropin-like proteins. The structure of phy3 LOV2 exhibits the characteristic PAS fold including the helix–turn–helix αA/

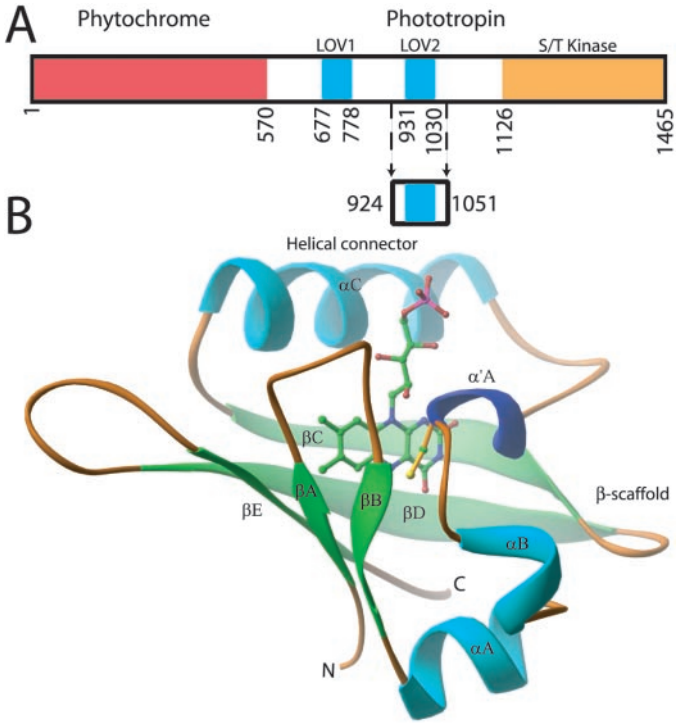

Fig. 1. *Adiantum* phy3 domain and LOV2 structures. (*A*) *Adiantum* phy3 domain structure showing the N-terminal phytochrome chromophore domain bound to a phototropin. Residues forming the LOV2 construct are marked by arrows. (*B*) RIBBON diagram of the phy3 LOV2 structure. The FMN cofactor is shown in the chromophore-binding pocket of LOV2 and is colored by elements: carbon, green; nitrogen, blue; oxygen, red; phosphorus, pink. C966 is at the N terminus of α′A and is colored yellow.

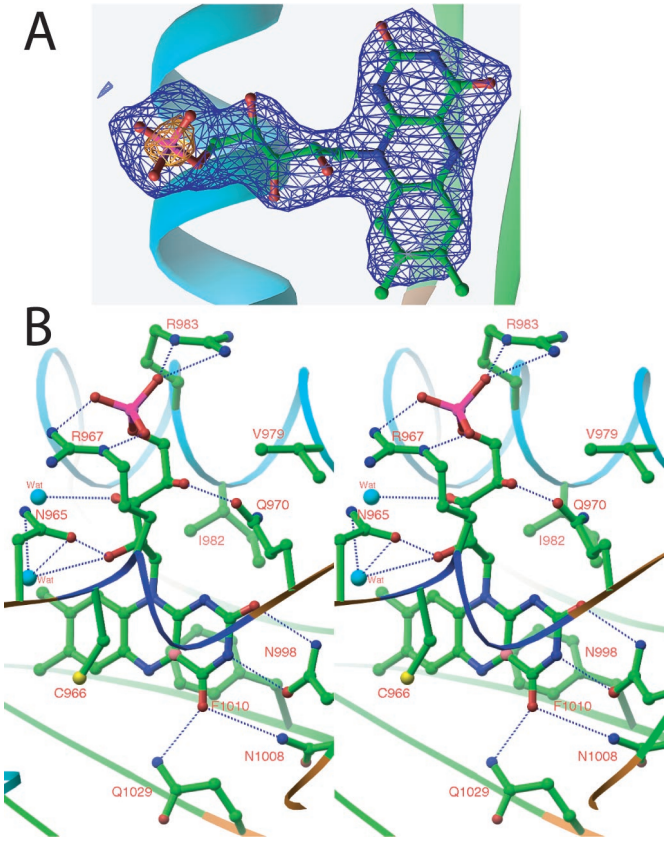

Fig. 2. Chromophore of phy3 LOV2. (*A*) Simulated-annealing omit map of FMN from one of the four monomers in the asymmetric unit. The map is contoured at $\pm 3.5\sigma$ (blue) and $\pm 10\sigma$ (yellow), in which σ is the rms-deviation value of the electron density. Electron density distinguishes the dimethylbenzene and pyrimidine moieties of the isoalloaxazine ring and shows a $+10\sigma$ feature over the terminal phosphate. (*B*) Stereo diagram of FMN–protein interactions. All residues and waters that hydrogen bond to or form van der Waals contact with FMN are shown. Hydrogen bonds are indicated by the dotted blue lines using a 2.6- to 3.5-Å range for hydrogen bonding. Atoms are colored as in Fig. 1 with the addition of sulfur as yellow, water molecules as light blue, and C(4a) of the isoalloxazine ring as pink.

αB, five-stranded β scaffold, and helical connector αC (ref. 15; Fig. 1*B*). A key region of secondary structure that varies in known PAS structures is the central helix, α′A. α′A is a single turn of a 3_{10} helix in LOV2 and HERG, an α-helix in FixL, and a π-helix in PYP.

A DALI (41) search of the phy3 LOV2 structure against known structures in the Protein Data Bank and comparison with known FMN proteins revealed no other FMN-binding PAS domains other than previously characterized LOV domains. Although the PAS domains of nitrogen fixation regulatory protein L and *E. coli* aerotaxis sensor are predicted to contain flavin adenine dinucleotide (27–29), their structures have not been determined.

Characterization of Flavin-Binding Pocket. A single molecule of FMN is bound noncovalently in the interior of the LOV2 domain by a network of hydrogen bonds and van der Waals and electrostatic interactions. Residues in the α′A helix and β-strands C, D, and E make the majority of flavin contacts (Fig. 2*B*). The flavin-binding pocket is primarily polar on the pyrimidine side of the isoalloxazine ring and nonpolar around the dimethylbenzene moiety. The ribityl chain of FMN is in the gauche conformation with respect to its 2′ and 3′ OH and terminates at the surface of LOV2, on which the phosphate interacts with the guanidinium groups of R983 and R967, forming salt bridges. Side-chain carbonyl oxygen atoms of N965 and Q970 are positioned 2.8 and 3.3 Å from the 2′ and 4′ hydroxyl groups of the ribityl chain forming hydrogen bonds. Hydrogen bonding between the isoalloxazine ring and the protein occurs through the side chains of N998, N1008, and Q1029. The side-chain carbonyl oxygen and amide nitrogen of N998 are 2.9 and 3.0 Å from N3 and O2 of FMN, respectively; the amide nitrogens of N1008 and Q1029 are both 3.4 Å from O4. Residues making van der Waals contact with the ribityl moiety are V979 with the 4′ hydroxyl and I982 with C1. F1010 is stacked on the *re* face of the isoalloxazine ring where C_ε contacts N5. Residues V986, L1012, F1025, T934, and V932 (not shown in Fig. 2*B*) define the hydrophobic pocket around the dimethylbenzene moiety. Additionally, two buried water molecules are located in equivalent positions in the flavin-binding pocket in all four LOV2 monomers within the asymmetric unit. One forms a hydrogen bond to the 2′ hydroxyl group of the ribityl chain and the other to the 3′ hydroxyl; both form hydrogen bonds to the side chain of N965.

Interestingly, there is no hydrogen bond to the N5 atom of the isoalloxazine ring; the closest prospective hydrogen-bond donor is the side chain of Q1029, which is 3.6 Å away. A hydrogen bond to N5 is a recurrent feature in most flavoenzymes (42) but is absent in vannilyl-alcohol oxidase (43) and glycolate oxidase (44). Although both of these flavoproteins exhibit a higher-than-average redox potential (45, 46), the consequences of the absence of a hydrogen bond at this position are not clear.

Importantly, the C_β of the buried C966 makes van der Waals contact with the ribityl 2′ hydroxyl and flanks the *si* face of the flavin ring. Spectroscopic and mutational analyses on LOV1

BIOCHEMISTRY

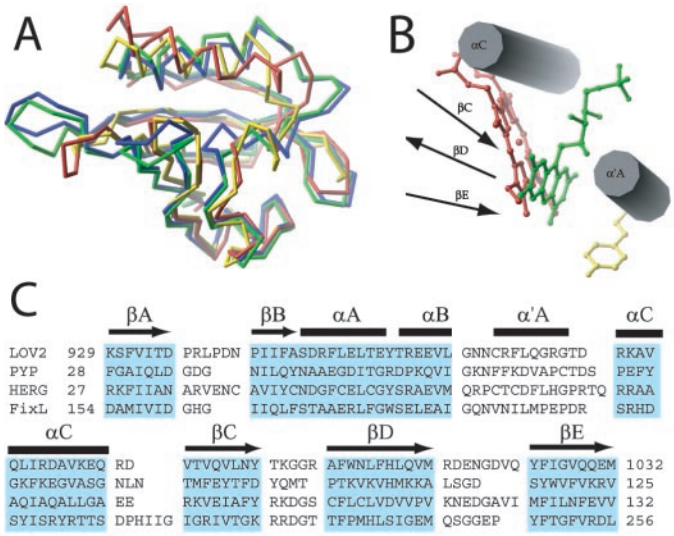

Fig. 3. Structural alignment of four PAS domains. (*A*) Least-squares superposition: FixL, red; PYP, yellow; HERG, blue; phy3 LOV2, green. (*B*) Comparison of positions of phy3 LOV2 (green), FixL (red), and PYP (yellow) chromophores within the chromophore-binding pocket of PAS domain. The secondary structural elements are represented schematically as cylinders and arrows. (*C*) Structure-based alignment of the sequences of these four PAS domains. Residues boxed in blue form secondary structural elements conserved among all four structures. These residues were used to optimize the least-squares fit shown in Fig. 3*A*. Secondary structure is noted above the alignment: β-strand, arrows; helix, bars.

and LOV2 domains in solution (13) have shown that this cysteine (corresponding to C39 in ref. 13) is not essential for flavin binding but is essential for the reversible photochemical reaction. Dark-minus-light difference absorption spectra suggest the formation of a C(4a)-cysteinyl adduct after absorption of light in both domains (13). In the LOV2 structure, the S_γ of C966 is 4.2 Å from C(4a). Facile rotation around the C_α–C_β bond would bring S_γ within 2.6 Å of C(4a) and promote the light-induced formation of a covalent flavin-cysteinyl adduct between C966 and C(4a), as suggested by this structural model.

Comparison of LOV2 to Other PAS Domains. The three known structures in the PAS superfamily share the same general fold as LOV2 (Fig. 3*A*). Pairwise alignment of the four PAS sequences in Fig. 3*C* shows that no two sequences exceed 20% identity except for HERG and phy3 LOV2, which are 30% identical. A least-squares fit of the LOV2 structure against these domains excluding the loop regions and by using only the highlighted residues in a secondary structure-based alignment (Fig. 3*C*) gave rms-deviation values of 1.5 Å for HERG, 2.6 Å for PYP, and 3.2 Å for FixL, which confirms the high structural homology between these domains in the absence of high sequence homology (Fig. 3*A*). However, comparison of the position of the bound LOV2, PYP, and FixL cofactors demonstrates substantial variability in cofactor binding (Fig. 3*B*). The 4-hydroxycinnamic acid of PYP is positioned outside the central portion of the fold and extends down toward αA/αB (helices not shown). The heme of FixL and the FMN of LOV2 both occupy the central part of the fold and interact with βD and βE, but these cofactors are inclined to each other at $\approx$30° and protrude from the chromophore-binding pocket on opposite sides of the connector helix αC. The propionate groups of heme are positioned at the surface of FixL between αC and βC, but the ribityl chain and terminal phosphate of FMN in phy3 LOV2 extend to the protein surface between αC and α'A. Thus, the same basic protein fold binds chemically diverse cofactors in the same general region but in very different ways.

The phy3 LOV2 structure provides strong additional evidence that PAS domains retain a conserved structure despite low overall sequence homology and display extensive functional diversity. The fact that quite distinct PAS sequences from a range of higher and lower taxa retain the same fold suggests that this domain is an evolutionarily conserved key signal-transduction component. While structure has been conserved sequence has evolved, enabling the domain to bind disparate cofactors (or none), to respond to a range of external stimuli, and to function in diverse signal-transduction pathways.

Alignment of Flavin-Interacting Residues. To assess the conservation of flavin-interacting residues in LOV domains, a multiple sequence alignment was generated containing the LOV1 and LOV2 domains of phototropins from three different plant species (Fig. 4). The high degree of sequence conservation among the LOV1 and LOV2 domains suggests that they possess an identical fold. In particular, the 11 residues that interact with FMN in phy3 LOV2 (Fig. 4) are conserved in all aligned phototropin LOV domains with the exception of residue 1,010, which is phenylalanine in all LOV2 and a leucine in all LOV1 domains. This sequence conservation is retained in other phototropins including those from rice, corn, and the phototropin-like proteins, rice NPH1b, and *Arabidopsis* NPL1 (refs. 47 and 48; sequence data not shown). The nonconserved flavin-interacting residue, F1010, is one of several residues that are identical within the same LOV domain type but differ between LOV1 and LOV2. Salomon *et al.* (13) demonstrated that LOV1 and LOV2 from oat phototropin have different absorption spectra, fluorescence properties, and photoexcitation and recovery rates; the nature of the amino acid at position 1,010 may contribute to these differences.

A BLAST search against the phy3 LOV2 sequence revealed three additional proteins that possess almost all the conserved flavin-interacting residues found in the phototropins (Fig. 4). These three proteins are involved in circadian rhythm regulation and include *Arabidopsis* ztl (49) and fkf1 (50) and *Neurospora* Wc-1 (51, 52). Again, the high degree of sequence conservation suggests that these three proteins also possess a LOV-domain fold. The most conserved stretch in all the aligned LOV domains is the consensus sequence NCRFLQ, which constitutes the 3_{10} helix (α'A) in phy3 LOV2. The structurally unusual nature of this 3_{10}-helical region may contribute to the chemistry of photoactivation and subsequent downstream signaling. Moreover, the combination of conserved flavin-binding residues and the striking conservation of all residues in this helix, including the photochemically active cysteine, suggests that flavin-cysteinyl adduct formation may be a general molecular response to light both in phototropin and in these circadian rhythm-regulating proteins.

Proposed Model for Flavin-Cysteinyl Adduct Formation. Any model for the photocycle in LOV domains must account for the lack of reactivity in the dark and the light-activated formation of a transient covalent adduct between the catalytic cysteine and C(4a). The close proximity of the cysteine side chain to C(4a) noted above would favor nucleophilic attack of the cysteine thiolate anion on the isoalloxazine ring under certain conditions. Evidently, the pKa of the buried thiol is sufficiently high that there is only a small population of thiolate anions and hence, little or no cysteinyl-flavin adduct formation in the dark. However, the absorption of photons by the isoalloxazine ring causes a redistribution of electronic charges on the ring (53). Pariser–Parr–Pople and Pople–Segal complete neglect of differential overlap (CNDO) molecular orbital calculations on oxidized isoalloxazine predict that the basicity of N1 decreases

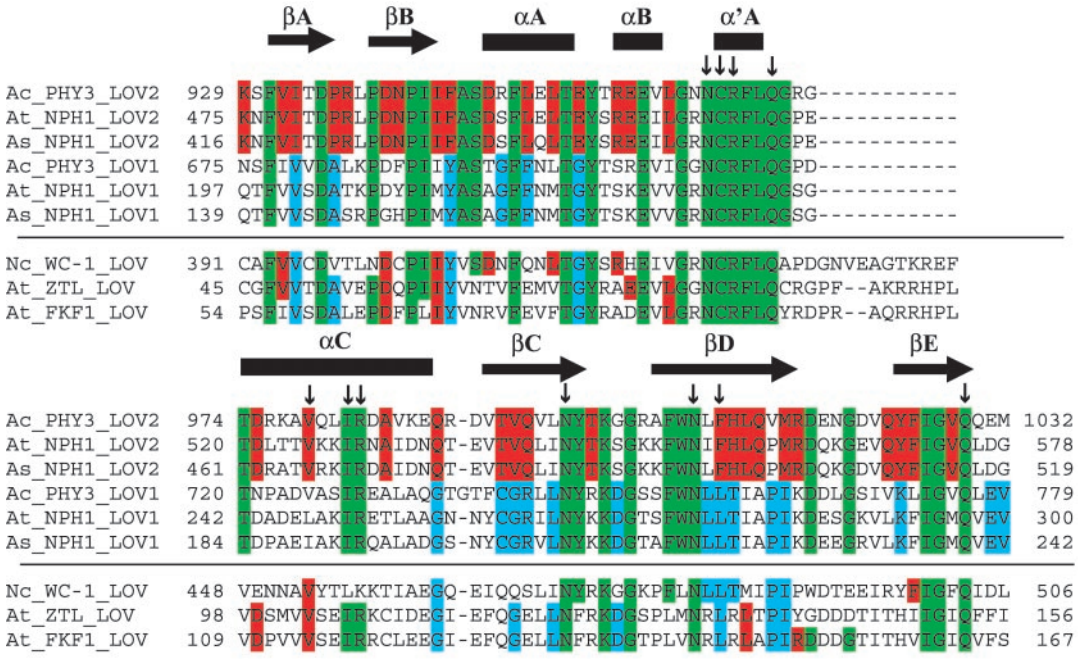

Fig. 4. Alignment of nine LOV-domain sequences and identification of flavin-interacting residues including LOV1 and LOV2 domains from *Adiantum* phy3 (GenBank accession no. BAA36192), *Arabidopsis* phototropin (GenBank accession no. AAC01753), oat phototropin (GenBank accession no. AAC05083), *Arabidopsis* ztl (GenBank accession no. AAF70288), *Arabidopsis* fkf1 (GenBank accession no. AAF32298), and *Neurospora* Wc-1 (GenBank accession no. Q01371). LOV2 residues that interact with FMN are marked with vertical arrows. Secondary structure of LOV2 is marked above alignment: β-strand, arrows; helix, bars. Green residues are conserved in all LOV1 and LOV2 domains included in the alignment as well as eight other LOV domains (not included because of space limitations) from rice phototropin (BAA84779), corn phototropin (T01353), rice phototropin-like protein nph1b (GenBank accession no. BAA84779) and *Arabidopsis* phototropin-like protein npl1 (GenBank accession no. AAC27293). Blue residues are conserved in all LOV1 domains, and red residues are conserved in all LOV2 domains from the above-listed proteins. This color scheme is applied to residues in Wc-1, ztl, and fkf1.

and that of N5 increases after photoexcitation to the lowest singlet and triplet excited states (54). Thus, photoexcitation of FMN in LOV2 could alter the electronic state of the isoalloxazine ring, promote base abstraction of the thiol proton by N5, and nucleophilic attack of the thiolate anion on C(4a) to create the cysteinyl-flavin adduct. A concerted mechanism in which N5 is protonated as the thiol sulfur attacks C(4a) may be more favorable, because it would eliminate the formation of a buried charge (Fig. 5). Adduct formation preceded by photoreduction of flavin presumably would reduce flavin electrophilicity, and hence the likelihood of nucleophilic attack by the cysteine thiolate. For this reason, reduction of the flavin may not be necessary for adduct formation. Dark-state recovery of the flavin adduct may be driven thermally or protein assisted. Time-resolved crystallographic studies (55, 56) should reveal important details in this process.

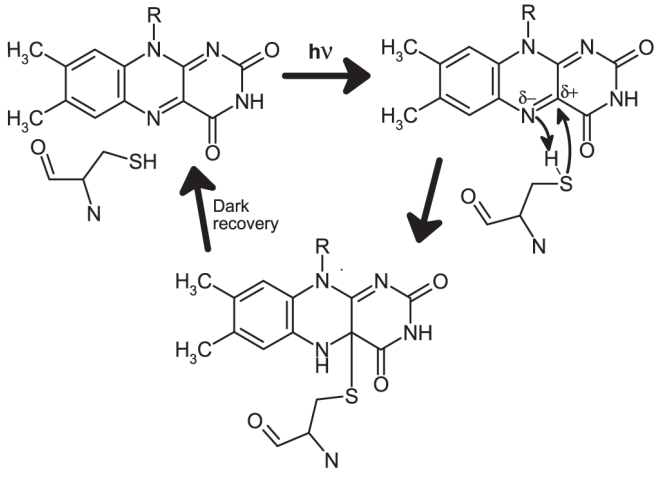

Fig. 5. Proposed schematic mechanism for cysteine-C(4a) covalent adduct formation in response to light absorption by the LOV domain (see text).

Conserved Surfaces and Signal Transduction. Mapping the sequence alignment of the LOV domains (Fig. 4) on to a space-filling model of phy3 LOV2 shows that the residues conserved in both LOV1 and LOV2 domains primarily cluster on a flat surface that contains the 3_{10}-helix α'A and the photoactive cysteine (Fig. 6), residues that are likely to move during photoexcitation and subsequent adduct formation. It has been demonstrated that LOV domains from Wc-1 will homodimerize specifically *in vitro* (51). The highly conserved

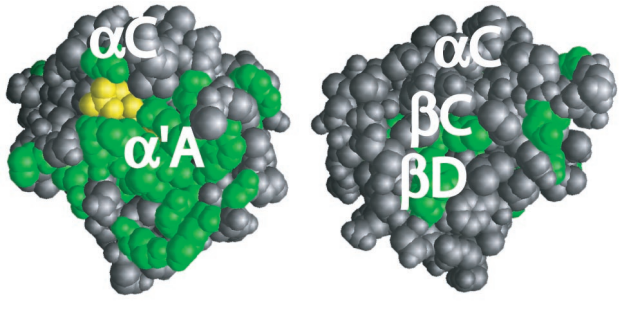

Fig. 6. Space-filling model of phy3 LOV2 showing the surface position of residues conserved in all LOV1 and LOV2 domains (green). Terminal phosphate of FMN is colored yellow. (*Left*) Model of the conserved face containing the 3_{10}-helix α'A. (*Right*) Model is rotated 180° about a vertical axis in the plane of Fig. 1.

BIOCHEMISTRY

surface in phototropin LOV domains may form a LOV interdomain-dimerization interface between LOV1 and LOV2 domains in a single phototropin molecule or between distinct molecules within a signaling complex. Phototropin may form part of a scaffold-protein-mediated signaling complex (57) in which multiple phototropin molecules are present (58). The absorption of light may regulate the presence or absence of LOV dimers within a signaling complex and in turn the function of the C-terminal kinase. Conversely, the conserved surface of phototropin LOV domains may interact directly with the kinase and regulate its activity. Structural studies on full-length phototropin may provide insight into the mechanism of kinase regulation and signaling.

We thank Carl Correll, Phoebe Rice, Xiaojing Yang, and Vukica Šrajer for providing invaluable assistance during the process of solving this structure and Marius Schmidt, Wouter Hoff, and Marvin Makinen for helpful discussion. We thank Winslow Briggs and John Christie for introducing us to this system, for generously providing the phy3 construct, and for numerous helpful discussions. Supported by National Institutes of Health Grant GM36452 to K.M. and a National Science Foundation Predoctoral Fellowship to S.C.

1. Singhal, G. S., Renger, G., Sopory, S. K., Irrgang, K.-D. & Govindjee (1999) in *Concepts in Photobiology: Photosynthesis and Photomorphogenesis* (Kluwer, Boston), pp. 775–929.
2. Batschauer, A. (1998) *Planta* **206,** 479–492.
3. Briggs, W.R. & Huala, E. (1999) *Annu. Rev. Cell Dev. Biol.* **15,** 33–62.
4. Fankhauser, C. & Chory, J. (1999) *Curr. Biol.* **9,** 123–126.
5. Cashmore, A. R., Jarillo, J. A., Wu, Y. J. & Liu, D. M. (1999) *Science* **284,** 760–765.
6. Frechilla, S., Zhu, J., Talbott, L. D. & Zeiger, E. (1999) *Plant Cell Physiol.* **40,** 949–954.
7. Huala, E., Oeller, P. W., Liscum, E., Han, I.-S., Larsen, E. & Briggs, W. R. (1997) *Science* **278,** 2120–2123.
8. Lasceve, G., Leymarie, J., Olney, M. A., Liscum, E., Christie, J. M., Vavasseur, A. & Briggs, W. R. (1999) *Plant Physiol.* **120,** 605–614.
9. Christie, J. M., Reymond, P., Powell, G. K., Bernasconi, P., Raibekas, A. A., Liscum, E. & Briggs, W. R. (1998) *Science* **282,** 1698–1701.
10. Nozue, K., Kanegae, T., Imaizumi, T., Fukuda, S., Okamoto, H., Yeh, K.-C., Lagarias, J. C. & Wada, M. (1998) *Proc. Natl. Acad. Sci. USA* **95,** 15826–15830.
11. Wada, M. & Sei, H. (1994) *J. Plant Res.* **107,** 181–186.
12. Christie, J. M., Salomon, M., Nozue, K., Wada, M. & Briggs, W. R. (1999) *Proc. Natl. Acad. Sci. USA* **96,** 8779–8783.
13. Salomon, M., Christie, J. M., Knieb, E., Lempert, U. & Briggs, W. R. (2000) *Biochemistry* **39,** 9401–9410.
14. Miller, S. M., Massey, V., Ballou, D., Williams, C.H., Jr., Distefano, M. D., Moore, M. J. & Walsh, C. T. (1990) *Biochemistry* **29,** 2831–2841.
15. Pellequer, J.-L., Wager-Smith, K. A., Kay, S. A. & Getzoff, E. D. (1998) *Proc. Natl. Acad. Sci. USA* **95,** 5884–5890.
16. Zhulin, I. B., Taylor, B. L. & Dixon, R. (1997) *Trends Biochem. Sci.* **22,** 331–333.
17. Ponting, C. P. & Aravind, L. (1997) *Curr. Biol.* **7,** R674–R677.
18. Taylor, B. L. & Zhulin, I. B. (1999) *Microbiol. Mol. Biol. Rev.* **63,** 479–506.
19. Borgstahl, G. E., Williams, D. R. & Getzoff, E. D. (1995) *Biochemistry* **34,** 6278–6287.
20. Genick, U. K., Borgstahl, G. E., Ng, K., Ren, Z., Pradervand, C., Burke, P. M., Šrajer, V., Teng, T.-Y., Schildkamp, W., McRee, D. E., *et al.* (1997) *Science* **275,** 1471–1475.
21. Gong, W., Hao, B., Mansy, S. S., Gonzalez, G., Gilles-Gonzalez, M. A. & Chan, M. K. (1998) *Proc. Natl. Acad. Sci. USA* **95,** 15117–15182.
22. Miyatake, H., Mukai, M., Park, S.-Y., Adachi, S.-I., Tamura, K., Nakamura, K., Tsuchiya, T., Iizuka, T. & Shiro, Y. (2000) *J. Mol. Biol.* **301,** 415–431.
23. Cabral, J. H. M., Lee, A., Cohen, S. L., Chait, B. T., Li, M. & Mackinnon, R. (1998) *Cell* **95,** 649–655.
24. Hoff, W. D., Düx, P., Hard, K., Nugteren-Roodzant, I. M., Crielaard, W., Boelens, R., Kaptein, R., van Beeumen, J. & Hellingwerf, K. J. (1994) *Biochemistry* **33,** 13959–13962.
25. Baca, M., Borgstahl, G. E., Boissinot, M., Burke, P. M., Williams, D. R., Slater, K. A. & Getzoff, E. D. (1994) *Biochemistry* **33,** 14369–14377.
26. Gilles-Gonzalez, M. A., Ditta, G. S. & Helinski, D. R. (1991) *Nature (London)* **350,** 170–172.
27. Soderback, E., Reyes-Ramirez, F., Eydmann, T., Austin, S., Hill, S. & Dixon, R. (1998) *Mol. Microbiol.* **28,** 179–192.
28. Bibikov, S. I., Biran, R., Rudd, K. E. & Parkinson, J. S. (1997) *J. Bacteriol.* **179,** 4075–4079.
29. Rebbapragada, A., Johnson, M. S., Harding, G. P., Zuccarelli, A. J., Fletcher, H. M., Zhulin, I. B. & Taylor, B. L. (1997) *Proc. Natl. Acad. Sci. USA* **94,** 10541–10546.
30. Otwinowski, Z. & Minor, W. (1997) *Methods Enzymol.* **276,** 307–326.
31. Navaza, J. (1994) *Acta. Crystallogr. A* **50,** 157–163.
32. Bailey, S. (1994) *Acta. Crystallogr. D* **50,** 760–763.
33. Brunger, A. T., Adams, P. D., Clore, G. M., DeLano, W. L., Gros, P., Grosse-Kunstleve, R. W., Jiang, J. S., Kuszewski, J., Nilges, M., Pannu, N. S., *et al.* (1998) *Acta. Crystallogr. D* **54,** 905–921.
34. Jones, T. A., Zou, J. Y., Cowan, S. W. & Kjeldgaard, M. (1991) *Acta. Crystallogr. A* **47,** 110–119.
35. Laskowski, R. A., MacArthur, M. W., Moss, D. S. & Thornton, J. M. (1993) *J. Appl. Crystallogr.* **26,** 283–291.
36. Carson, M. (1997) *Methods Enzymol.* **277,** 493–505.
37. Kleywegt, G. J. & Jones, T. A. (1995) *Structure (London)* **3,** 535–540.
38. Kleywegt, G. J. & Jones, T. A. (1996) *Acta. Crystallogr. D.* **52,** 826–828.
39. Smith, R. F., Wiese, B. A., Wojzynski, M. K., Davison, D. B. & Worley, K. C. (1996) *Genome Res.* **6,** 454–462.
40. Nicholls, A., Sharp, K.A. & Honig, B. (1991) *Proteins* **11,** 281–296.
41. Holm, L. & Sander, C. (1993) *J. Mol. Biol.* **233,** 123–138.
42. Fraaije, M. W. & Mattevi, A. (2000) *Trends Biochem. Sci.* **25,** 126–132.
43. Fraaije, M. W., van den Heuvel, R. H. H., van Berkel, W. J. H. & Mattevi, A. (2000) *J. Biol. Chem.* **275,** 38654–38658.
44. Lindqvist, Y. (1989) *J. Mol. Biol.* **209,** 151–156.
45. van den Heuvel, R. H. H., Fraaije, M. W., Mattevi, A. & van Berkel, W. J. H. (2000) *J. Biol. Chem.* **275,** 14799–14808.
46. Pace, C. & Stankovich, M. (1986) *Biochemistry* **25,** 2516–2522.
47. Jarillo, J. A., Ahmad, M. & Cashmore, A. R. (1998) *Plant Physiol.* **117,** 719.
48. Kanegae, H., Tahir, M., Savazzini, F., Yamamoto, K., Yano, M., Sasaki, T., Kanegae, T., Wada, M. & Takano, M. (2000) *Plant Cell Physiol.* **41,** 415–423.
49. Somers, D. E., Schultz, T. F., Milnamow, M. & Kay, S. A. (2000) *Cell* **101,** 319–329.
50. Nelson, D.C., Lasswell, J., Rogg, L. E., Cohen, M. A. & Bartel, B. (2000) *Cell* **101,** 331–340.
51. Ballario, P., Talora, C., Galli, D., Linden, H. & Macino, G. (1998) *Mol. Microbiol.* **29,** 719–729.
52. Lee, K., Loros, J. J. & Dunlap, J. C. (2000) *Science* **289,** 107–110.
53. Song, P.-S. (1968) *J. Phys. Chem.* **72,** 536–542.
54. Song, P.-S. (1968) *Photochem. Photobiol.* **7,** 311–313.
55. Moffat, K. (1998) *Acta. Crystallogr. A* **54,** 833–841.
56. Perman, B., Anderson, S., Schmidt, M. & Moffat, K. (2000) *Cell. Mol. Biol.* **46,** 895–913.
57. Motchoulski, A. & Liscum, E. (1999) *Science* **286,** 961–964.
58. Reymond, P., Short, T. W. & Briggs, W. R. (1992) *Plant Physiol.* **100,** 655–661.